

A *Spitzer* search for cold dust within globular clusters

Pauline Barmby,^{1,2} Martha L. Boyer,³ Charles E. Woodward,³ Robert D. Gehrz,³ Jacco Th. van Loon,⁴ Giovanni G. Fazio,² Massimo Marengo,² Elisha Polonski⁵

ABSTRACT

Globular cluster stars evolving off the main sequence are known to lose mass, and it is expected that some of the lost material should remain within the cluster as an intracluster medium (ICM). Most attempts to detect such an ICM have been unsuccessful. The Multiband Imaging Photometer for *Spitzer* on the *Spitzer Space Telescope* was used to observe eight Galactic globular clusters in an attempt to detect the thermal emission from ICM dust. Most clusters do not have significant detections at $70\ \mu\text{m}$; one cluster, NGC 6341, has tentative evidence for the presence of dust, but $90\ \mu\text{m}$ observations do not confirm the detection. Individual $70\ \mu\text{m}$ point sources which appear in several of the cluster images are likely to be background galaxies. The inferred dust mass and upper limits are $< 4 \times 10^{-4} M_{\odot}$, well below expectations for cluster dust production from mass loss in red and asymptotic giant branch stars. This implies that either globular cluster dust production is less efficient, or that ICM removal or dust destruction is more efficient, than previously believed. We explore several possibilities for ICM removal and conclude that present data do not yet permit us to distinguish between them.

Subject headings: globular clusters: general — globular clusters: individual (NGC 104, NGC 362, NGC 1851, NGC 5272, NGC 5904, NGC 6205, NGC 6341, NGC 6752) — infrared: stars — stars: mass loss

¹Department of Physics & Astronomy, University of Western Ontario, London, ON N6A 3K7, Canada; e-mail: pbarmby@uwo.ca

²Harvard-Smithsonian Center for Astrophysics, 60 Garden Street, Cambridge, MA 02138

³Department of Astronomy, School of Physics and Astronomy, University of Minnesota, 116 Church St, SE, Minneapolis, MN 55455

⁴Astrophysics Group, Lennard Jones Laboratories, Keele University, Staffordshire, UK

⁵Department of Physics and Astronomy, University of Wisconsin Stevens Point, Stevens Point, WI 54481

1. Introduction

Post-main-sequence mass loss affects both present and future generations of stars. It determines the remnant state of stars of intermediate mass and below, as well as affecting the state and contents of the interstellar medium out of which new stars are formed. However, the rate and amount of mass lost by red giant branch (RGB) and asymptotic giant branch (AGB) stars is a major uncertainty in stellar evolutionary theory. As Origlia et al. (2007) and Catelan (2000) point out, existing formulations rely on empirical laws based on observations of Population I stars. There is little theoretical guidance on how mass loss should be included in stellar evolutionary models, or on how it affects population synthesis models based on the stellar models.

Globular clusters (GCs) have long been the prime testing grounds for stellar evolution theory. With large populations of low-mass stars of the same age, metallicity, and distance, they should be ideal places to test ideas about mass loss. There are several observational confirmations of the theoretical prediction that stars more massive than $0.8M_{\odot}$ lose a significant fraction of their mass after leaving the main sequence. These include initial-final mass estimates of white dwarfs (e.g. Kalirai et al. 2008) and evidence from line profiles of red giants (e.g., Meszaros et al. 2008). To explain the horizontal branch it was argued (e.g., Rood 1973) that much of this mass is shed on the RGB, but as AGB stars, post-AGB stars, and PNe are also observed in GCs (Alves et al. 2000; van Loon et al. 2007) some mass must be lost on the AGB as well. There is also ample observational evidence that many GCs have stars which are currently losing mass, at rates of $10^{-8} - 10^{-6}M_{\odot} \text{ yr}^{-1}$ (Ramdani & Jorissen 2001; Origlia et al. 2002; Boyer et al. 2006; Origlia et al. 2007; Ita et al. 2007). From these observations it is difficult to obtain an overall picture of time-averaged mass loss rates and duty cycles and their relation to cluster properties such as metallicity, since only a few stars at a time lose mass.

A more global picture of mass loss within GCs might be provided by the intra-cluster medium (ICM). Mass lost from GC stars is expected to accumulate in the ICM until the cluster passes through the Galactic disk, when the ICM will be stripped by ram pressure. The ICM is expected to be mostly gaseous (although the ionization state is unknown), with a small amount of dust formed in the extended atmospheres of red giants. The dust should be optically thin and heated by starlight to 50–80 K (Angeletti et al. 1982; Forte et al. 2002); its thermal emission should peak in the mid-to-far-infrared (IR) and could be detected as an IR excess at these wavelengths. Although GC stars are clearly losing mass, detections of the ICM have been surprisingly difficult. Searches for intra-cluster gas have been conducted for several decades (Birkinshaw et al. 1983; Roberts 1988; Faulkner et al. 1991; Freire et al. 2001; van Loon et al. 2006); searches for dust (Lynch & Rossano 1990; Knapp et al. 1995;

Origlia et al. 1996; Penny et al. 1997; Hopwood et al. 1999; Matsunaga et al. 2008) are more recent but have yielded similar results, mostly upper limits. Only one Galactic GC, NGC 7078 (M15), shows clear evidence for an infrared (IR) excess (Evans et al. 2003; Boyer et al. 2006). Diffuse infrared emission near NGC 6402 may be associated with the cluster or with Galactic cirrus, while NGC 5024 has an infrared point source which may be intracluster dust (Matsunaga et al. 2008). An additional cluster, NGC 6356, has a tentative detection of dust at submillimeter wavelengths (Hopwood et al. 1998). All of the detections imply dust masses well below the expected levels.

This paper presents results of a *Spitzer* (Werner et al. 2004; Gehrz et al. 2007) survey of eight Milky Way GCs using 24 and 70 μm observations with the Multiband Imaging Photometer for *Spitzer* (MIPS; Rieke et al. 2004). We describe our observational strategy and data analysis techniques in §2. Section 3 introduces our results, including the detection of excess IR emission in several of the target clusters and upper limits on the remaining clusters. Section 4 explores the implication of these new mid-IR results, including a comparison with predicted dust masses. We conclude in §5 with a summary and suggested follow-up observations.

2. Observations and data reduction

The target list (Table 1) comprises the Milky Way globular clusters that we believed to be the best candidates for ICM dust detection. These clusters are reasonably nearby, at high galactic latitude (to reduce confusing fore- and back-grounds), and have high escape velocities. They are among the most massive Galactic GCs. More massive clusters are more likely to harbor a larger number of stars in the short-lived superwind phase: if the ICM is being removed from the cluster on short time scales, then we are more likely to see it in a more massive cluster where the ICM material is being replenished more quickly. Clusters with escape velocities that are much larger than AGB wind speeds ($\sim 10 \text{ km s}^{-1}$) will also be more likely to retain ICM material. At the time this program was planned, all had existing or scheduled *Spitzer* mid-IR observations with the InfraRed Array Camera (IRAC; Fazio et al. 2004). Observing clusters with a range of times since last disk passage is desirable, but we did not use this as a selection criterion because orbital information is only available for a fraction of Milky Way globular clusters (e.g., from Odenkirchen et al. 1997). The clusters span a factor of thirty in metallicity (1.5 dex), important for testing the effects of metallicity on dust production and retention. All of the clusters are detected with IRAS (Knapp et al. 1995), and both NGC 104 (47 Tuc) and NGC 362 contain stars with known circumstellar dust (Origlia et al. 2002; Ita et al. 2007).

2.1. IRAC observations

IRAC photometry traces the Rayleigh-Jeans tail of the spectral energy distribution of globular cluster stars. Although cold intracluster dust is not expected to radiate at IRAC wavelengths, understanding the near-IR SED is very useful for quantifying any IR excess from the dust. IRAC observations of the clusters were made over the period 2005 July – 2006 September as part of *Spitzer* program identification (PID) 20298 (PI R. Rood), except for NGC 5904 which was part of PID 3256 (PI P. Goudfrooij). Dataset identifiers are given in Table 2. All but one of the clusters were observed in a single IRAC field of view ($5' \times 5'$) in all four channels, with 90–252 frames (12 s each) per position (30 frames, 30 s each for NGC 5904). NGC 104 was observed in a $5' \times 15'$ map. NGC 104 and NGC 6752 were observed in the high-dynamic-range (HDR) mode which includes short (0.6 s) frames taken before the 12 s frames. The half-light radius of NGC 104 ($190''$) is slightly too large to be fully covered by the PID 20298 observations. Fortunately, observations of this cluster covering a wider field of view were available, taken as part of instrument commissioning in 2003 November (PID 623). These observations were taken in 12-second HDR mode with 3 frames per position, and cover a $25' \times 30'$ area.

For all clusters, the *Spitzer* Science Center (SSC) pipeline version S14 post-BCD mosaics were used for integrated photometry. IRAF¹ *apphot* was used to measure integrated magnitudes within the half-light radii given in Table 1. For each cluster the background was measured in an annulus with inner and outer radii 108 and $117''$, respectively, and subtracted from the integrated magnitudes. For NGC 104 and NGC 6752, the mosaics made from the short-exposure frames were used to avoid bright star saturation; the other clusters had no saturation problems. The magnitudes measured in the half-light radii were converted to total flux densities with multiplication by 2, and corrected with application of the ‘extended source calibration’ given by the SSC. The results are given in Table 2, with electronic links to the observational data. The uncertainties in the flux densities due to Poisson noise from the cluster and sky background noise are very small ($< 0.5\%$); uncertainties in the absolute (a few percent; Reach et al. 2005) and extended source calibrations (10%) dominate the total flux measurements.

¹IRAF is distributed by the National Optical Astronomy Observatories, which are operated by the Association of Universities for Research in Astronomy, Inc., under cooperative agreement with the National Science Foundation.

2.2. MIPS observations

The MIPS Photometry Astronomical Observing Template (AOT) was used to produce $5' \times 5'$ images of the clusters at 24 and 70 μm . This field size is comparable to the cluster sizes (half-light radii from Harris 1996, $< 3'$). Although a somewhat larger field of view would have been desirable, this would have substantially increased the observing time. To set exposure times, we predicted the 24 and 70 μm stellar fluxes from the clusters' K_s -band fluxes (measured from 2MASS images; Nantais et al. 2006) assuming a Rayleigh-Jeans $f_\nu \propto \nu^2$ spectrum. The 24 μm observations were required to characterize the cluster SED, so high-significance detections of individual stars were not required. The estimated 24 μm flux was used to compute the expected average 24 μm surface brightness inside the clusters' half-light radii. The resulting values, 0.8–4.2 MJy sr^{-1} , were expected to be detectable in 1 cycle of the Photometry AOT with 10 second frame times. The intra-cluster dust is expected to emit most strongly at 70 μm ; however, even at this long wavelength, the integrated flux of the cluster stars is much brighter than the MIPS detection limits. We therefore targeted the exposure times to have strong detections of the integrated stellar photospheric flux; any dust signal would appear as an IR excess at 70 μm . The resulting predicted 70 μm fluxes ranged from 6–150 mJy, requiring 1–10 cycles of the MIPS Photometry AOT with 10 second frame times.

The observations were made over the period 2006 June – 2006 November under *Spitzer* PID 30031, a Guaranteed Time program of G. Fazio. The data were processed with the S14 version of the MIPS pipeline. Post-pipeline processing for the 24 μm BCD images included ‘self-calibration’ (dividing by the normalized median image of ‘off-source’ frames) and mosaicking; the 70 μm BCD images were time- and column-filtered and then mosaicked. All mosaicking used the MOPEX program (Makovoz & Khan 2005) with the standard parameters recommended in SSC documentation. The 24 μm mosaics have a pixel scale of $2.5''$, and the 70 μm mosaics have a scale of $5.0''$. Figures 1 and 2 show the cluster mosaic images. All of the clusters were detected at high signal-to-noise in the 24 μm images. The same is not true at 70 μm , and the major result of this paper is the lack of any strong dust signal from any of the eight clusters.

As for IRAC, flux densities in the MIPS bands were measured with aperture photometry. Inspection of Figure 1 shows that the mid-infrared light for several clusters (NGC 5272 and NGC 6205) appears to have slightly different centers from the optical centers given by Harris (1996). We computed new centers by smoothing the 24 μm images and computing the flux centroid of the smoothed images in a box of width 4 times the smoothed FWHM, centered on the optical center. The mid-IR centers are given in Table 3. Compared to the IRAC data, the choice of aperture for the MIPS images is less obvious: the intracluster medium

seems more likely to sink to the center of the cluster potential well than to follow the same spatial distribution as the cluster stars. [However, we note that both the extended emission detected in NGC 7078 by Boyer et al. (2006) and the possible intracluster dust in NGC 6024 reported by Matsunaga et al. (2008) are offset from the cluster centers.] We decided to use two apertures for each cluster: the optical half-light radius as for the IRAC data, and a smaller ‘core’ radius, to maximize signal-to-noise for detection of dust at the cluster center. The half-light radii are given in Table 1; for these apertures, background annuli with inner and outer radii 150 and 175'' were used. Following Carpenter et al. (2008), we chose a core aperture of 16'' radius (diameter twice the FWHM of the PSF), with background annuli 120–140'' in radius. To allow for subtraction of stellar contribution to the 70 μm signal (see §3.2), the 24 μm photometry in this aperture was measured on versions of the images convolved to the 70 μm resolution using a kernel described in Gordon et al. (2008).

The results of the aperture photometry are listed in Table 3, with electronic links to the observational data; no color corrections have been made to these values. The only aperture correction made is a multiplicative factor of 1.13 applied to the large-aperture 70 μm photometry. Again following Carpenter et al. (2008), uncertainties in the MIPS flux density were calculated as

$$\sigma = \eta_{\text{corr}} \eta_{\text{sky}} \sigma_{\text{sky}} \sqrt{N_{\text{ap}} + N_{\text{ap}}^2 / N_{\text{sky}}} \quad (1)$$

where η_{corr} accounts for the noise correlation between pixels due to re-sampling during mosaicing ($\eta_{\text{corr}} = 1$ for 24 μm and 2 for 70 μm), η_{sky} is discussed below, σ_{sky} is the standard deviation of the pixels in the background annulus, and N_{ap} and N_{sky} are the number of pixels in the photometry and background apertures, respectively. (Poisson noise from the clusters is negligible compared to the background noise.) After examining noise in their 70 μm background and photometry apertures, Carpenter et al. (2008) concluded that ‘excess noise’ corresponding to $\eta_{\text{sky}} = 1.5$ was present in their photometry apertures, a conclusion validated by their distribution of signal-to-noise ratios. Although this precise value may not apply to our observations, which were made in a slightly different manner, we adopt it here to be conservative. The uncertainties in Table 3 do not include uncertainties in the absolute calibration (2% at 24 μm and 5% at 70 μm ; Gordon et al. 2007; Engelbracht et al. 2007).

Confusion noise due to extragalactic sources is not expected to affect these observations: Frayer et al. (2006) derived the 70 μm confusion limit due to extragalactic sources as 0.3 mJy, well below the flux regime of the observations presented here. Confusion due to Galactic cirrus, however, is an issue: Jeong et al. (2005) computed the MIPS 70 μm point source detection limits due to Galactic cirrus confusion at the latitudes of our clusters ($|b| > 27$) as 0.1 – 0.2 mJy, again below our detection limits. For larger apertures, however, the confusion noise and detection limits scale as $d^{1-\alpha/2}$ where d is the aperture size and $\alpha \approx -3.5$ is the

cirrus power spectrum index. The scaling factors range from about 6 to several hundred for the half-light radius apertures used, and hence cirrus confusion will affect our ability to detect extended emission for clusters with large angular sizes.

3. Analysis

3.1. Cluster spectral energy distributions

Figure 3 shows the cluster spectral energy distributions (SEDs) from 0.3 to 100 μm . The new IRAC measurements from Table 2 and half-light radius MIPS measurements from Table 3 (multiplied by 2 to convert to total fluxes, even though this may not be appropriate for non-stellar emission) are shown as filled symbols. Also plotted are extinction-corrected total optical and near-IR magnitudes given by Harris (1996) and Cohen et al. (2007). IRAS measurements from the Faint Source Catalog (Knapp et al. 1995) are also shown; the 12 and 25 μm measurements have been corrected for the cluster extent following the procedure used by Knapp et al. (1995) and flux densities in all IRAS bands have been color-corrected using the values for a 5000 K blackbody given in the *IRAS Explanatory Supplement*. Upper limits to the 90 μm flux densities given by Matsunaga et al. (2008) are shown for the five clusters in common between the two samples. Overplotted are black-body SEDs derived from fits to the flux densities (equally-weighted) at $\lambda < 5 \mu\text{m}$. All are consistent with the expected average temperatures for globular cluster stars (4500–5500 K).

A first check of our measurements is to compare them with previous work. The *Spitzer* and IRAS results are mutually consistent except for NGC 6341, where the 70 μm data are slightly above the IRAS 60 μm upper limits. We suggest that the IRAS limit might be slightly too low if there is extended emission from the cluster. For NGC 104, both the 60 and 70 μm observations are below the predictions based on the black-body fit, possibly because of the large spatial extent of the cluster. Two of our target clusters were observed with the PHOT instrument on ISO by Hopwood et al. (1999): using those authors’ method to convert surface brightness to flux density, their derived 70 μm flux densities are $130 \pm 50 \text{ mJy}$ for NGC 104 and $220 \pm 90 \text{ mJy}$ for NGC 7252. Our measurements for these clusters are consistent with these values. The 70 μm measurements are generally consistent with the 90 μm upper limits given by Matsunaga et al. (2008), except for NGC 6341, where the 70 μm value appears to be too large. The detection for this cluster is at $< 3\sigma$ significance and may be spurious.

Figure 4 compares the predicted (from the black-body fit) and measured flux densities (the same values as in the previous figure) at 24 and 70 μm . We expected that any ICM dust would likely be too cool to be detectable at 24 μm ; however, circumstellar dust should

be warmer and possibly detected at this wavelength. All of the $24\ \mu\text{m}$ flux densities are within 20% of the prediction; six clusters are within 10%. This is reasonable accuracy considering the difficulties in deriving integrated measurements of these resolved objects. The non-detection of $24\ \mu\text{m}$ excesses in integrated photometry may simply reflect the small number of mass-losing AGB stars compared to the bulk of the population. Point-spread-fitting photometry of the $24\ \mu\text{m}$ images, while beyond the scope of this work, may reveal which stars are surrounded by circumstellar dust. Seven of the eight clusters in the sample have measurements or upper limits on $70\ \mu\text{m}$ flux that are more than a factor of 2 above the black-body prediction. The exception is NGC 104, for which the $70\ \mu\text{m}$ upper limit is *lower* than the predicted photospheric value. The problem could be background subtraction: the half-light radius is almost as large as the $70\ \mu\text{m}$ image and a “background” region is difficult to define.

3.2. Non-stellar fluxes at $70\ \mu\text{m}$

Figures 3 and 4 clearly demonstrate that only one of the clusters in our sample—NGC 6341—has a significant infrared excess. To quantify this, we computed (limits on) the $70\ \mu\text{m}$ non-stellar emission in both the half-light and core apertures. To compute the non-stellar emission in the half-light aperture, we assumed that any photospheric emission at $70\ \mu\text{m}$ follows the optical emission, i.e., half of the total emission is contained within R_h . As an estimate of the stellar emission at $70\ \mu\text{m}$ we use the predicted value from the black-body fit described above. Thus the non-stellar emission at $70\ \mu\text{m}$ in the half-light radius is

$$f_{70,\text{ns}} = f_{70,\text{obs}} - 0.5 \times f_{70,\text{pred}}. \quad (2)$$

The fraction of stellar emission contained within the core aperture is not as straightforward to compute; to estimate it, we scale the flux measured at $24\ \mu\text{m}$ in the core aperture (recall that the image used to measure this flux was convolved to the $70\ \mu\text{m}$ resolution) by the ratios of the predicted total fluxes at 70 and $24\ \mu\text{m}$. Therefore the non-stellar emission at $70\ \mu\text{m}$ in the core aperture is:

$$f_{70,\text{ns}} = 1.76[f_{70,\text{obs}} - (f_{24,\text{obs}}/f_{24,\text{pred}}) \times f_{70,\text{pred}}] \quad (3)$$

where the factor of 1.76 is the aperture correction for a point source measured in a $16''$ aperture. Table 4 gives the derived non-stellar fluxes for each cluster, together with the dust mass predictions and observational limits derived in §4.1.

Only one cluster shows even tentative evidence for the detection of excess IR emission at $70\ \mu\text{m}$: NGC 6341. Figure 2 shows that the apparent $70\ \mu\text{m}$ emission in this cluster

comes from an extended region offset from the cluster core by roughly 43 arcsec, or about $(2/3)R_h$. Within the emission region there are three separate peaks which contain about 60% of the total flux; it is unclear whether these peaks are separate point sources (none has a co-located 24 μm source) or merely represent structure in the emission. In comparison, the dust emission detected in NGC 7078 by Boyer et al. (2006) is much rounder and is located closer to the center of that cluster ($\sim R_h/4$); however, the possible dust cloud in NGC 5024 detected by Matsunaga et al. (2008) is also far from the cluster center, at $0.8R_h$. The IRIS 60 μm sky maps do show some nebulosity near NGC 6341, so it is possible that the detected flux is in fact not associated with the cluster; however NGC 1851, at a similar Galactic latitude, also has some nearby nebulosity and does not have a 70 μm detection. Future data from the Akari All-Sky Survey should have sufficient spatial resolution to address the issue of whether there is diffuse emission near NGC 6341. The lack of any excess infrared emission in the 90 μm Akari observations of NGC 6341 by Matsunaga et al. (2008) (see Fig. 3) casts doubt on the reality of our low-significance detection; however, we retain it for analysis in the remainder of this paper.

3.3. Point sources detected at 70 μm

While only some of the clusters have spatially diffuse IR emission within R_h , all of the 70 μm images except those of NGC 104 and NGC 5904 do contain some faint point sources which are not concentrated toward the cluster centers. [Most of the point sources identified by Matsunaga et al. (2008) are off the fields of view of our images.] What is the nature of these sources? The 70 μm data provide only marginal detections and poor spatial localization, but the 24 μm data provide additional clues to the nature of the sources.

Initially, visual examination was used to generate lists of possible point sources in each cluster image. Using an estimated 70 μm position as a starting point, we performed aperture photometry on the 24 and 70 μm images using IRAF/phot, with the photometry routine allowed to re-center the sources. Several 70 μm sources were off the edges of the 24 μm images, or not visible at the shorter wavelength: the latter group could either be very red sources, or noise fluctuations in the 70 μm images. Standard photometric apertures as given in the MIPS Data Handbook were used (at 70 μm , aperture radius 18'' and background annulus 39 – 65''; at 24 μm , aperture radius 6'' and background annulus 20 – 32'') and appropriate aperture corrections were applied. We did not attempt IRAC photometry for the 70 μm sources: the IRAC images of the GCs are significantly more crowded, and we were doubtful about the reliability of measurements in these regions.

The 70 μm sources in the globular cluster fields could be stars within the cluster, un-

related Galactic stars, or background galaxies. To discriminate between these possibilities, a color-magnitude diagram was made from the MIPS photometry, shown in Figure 5. For comparison, the AGB and post-AGB models (restricted to oxygen-rich models with $\dot{M} \leq 10^{-6} M_{\odot}$, which are most appropriate for comparison with GCs) of Groenewegen (2006) are also shown. The model fluxes have been scaled down by a factor of 5 to reflect a dust-to-gas ratio appropriate for GC metallicities. The model fluxes are scaled to a common fiducial distance (8.5 kpc) so the same practice was followed for the cluster sources. In addition to the evolved star models, we show the (unscaled) flux densities and ratios for 70 μm sources in the ELAIS-N2 field of the SWIRE Legacy Survey (Lonsdale et al. 2003); these sources are predominantly extragalactic. All but one of the cluster field 70 μm sources are very red, with typical values of $f_{70}/f_{24} \approx 10$, compared to the Rayleigh-Jeans value of ~ 0.1 . The cluster source colors are more similar to those of the galaxies than to most of the evolved-star models, and the stellar models with similar colors are significantly brighter.

From the colors, we tentatively conclude that the 70 μm sources in the cluster fields are likely background galaxies. The high Galactic latitude of the clusters ($|b| > 26^\circ$) supports this conclusion, as do the results of Boyer et al. (2008) from their study of 70 μm sources near ω Cen and those of Matsunaga et al. (2008). The number density of sources is also consistent with this conclusion: there are 23 sources in a total of 346 arcmin² for a density of 0.066 arcmin⁻². The number counts given by Frayer et al. (2006) for the GOODS-North field show that there are 0.07 galaxies arcmin⁻² to flux limits of 11 mJy (appropriate for our average field), comparable to the number in the cluster fields. Ita et al. (2007) observed NGC 104 and 362 at mid-infrared wavelengths from 2.4–24 μm . Those authors found eight red sources ($F_{24}/F_7 > 1$) in NGC 362; no such sources were found in NGC 104. Comparing our images of NGC 362 to those of Ita et al. (2007), we find that their red sources A, D and F are within our field of view. Only source D is detected at 70 μm ; it has $F_{70}/F_{24} \approx 15$, consistent with the colors of a galaxy.

4. Discussion

4.1. Dust masses and limits

The non-stellar 70 μm fluxes computed in §3.2 allow us to estimate the amount of dust present in these clusters. For the clusters with negative non-stellar fluxes, we computed the dust mass upper limits as $3\sigma_{\text{flux}}$. We follow Evans et al. (2003) in assuming any dust to be optically thin, so the dust mass is given by:

$$\frac{M_d}{M_{\odot}} = 4.79 \times 10^{-17} f_{\nu} [\text{mJy}] \frac{D_{\text{kpc}}^2}{\kappa_{\nu} B_{\nu}(T_d)} \quad (4)$$

where κ_ν is the dust absorption coefficient and $B_\nu(T_d)$ the Planck function, both in cgs units. Our data do not constrain the dust temperature, so we use the value found by Boyer et al. (2006) for NGC 7078 ($T_d = 70$ K), and the same $\kappa_\nu = 56 \text{ cm}^2 \text{ g}^{-1}$. Different assumptions about these two quantities can change the derived dust masses by several orders of magnitude; for example, Evans et al. (2003) estimated the dust mass in NGC 7078 by using κ for amorphous fayalite at 50 K; at 70 μm this substance has $\kappa = 280 \text{ cm}^2 \text{ g}^{-1}$, or five times the value used by Boyer et al. (2006). On the opposite extreme, Knapp et al. (1995) assume silicate grains with $T = 45$ K; with $\kappa_\nu \propto \nu$, the absorption coefficient at 70 μm is $36 \text{ cm}^2 \text{ g}^{-1}$. Table 5 of Hopwood et al. (1999) shows the effects of different assumptions about the dust temperature on derived dust masses: changing from $T_d = 70$ K to $T_d = 40$ K, for the same composition, increases the inferred M_d by about a factor of ten, while increasing from $T_d = 70$ K to $T_d = 100$ K decreases M_d by about a factor of 2.5. Uncertainties in the dust composition and temperature therefore result in uncertainties of $\lesssim 2$ orders of magnitude in derived dust masses.

Table 4 gives the dust mass upper limits derived from the 70 μm measurements in both the half-light and core apertures. All values reported are 3σ upper limits, except for the possible (2.2σ) detection of total dust mass in NGC 6341. This is our only observation resulting in even a tentative detection; we show it as a value rather than an upper limit in the table and following plots in order to give a visual estimate of the uncertainties. Because the cluster emission is generally very faint, we have not attempted to subtract any point source emission from the total fluxes; if point sources within the apertures are unrelated to the clusters then the true upper limits would be even lower. For all of the clusters in our sample, the limits on the total dust masses are $< 4 \times 10^{-4} M_\odot$; the limits on core masses are an order of magnitude lower, $< 4 \times 10^{-5} M_\odot$. Hopwood et al. (1999) gave upper limits to the dust masses for NGC 104 and NGC 5272; our total value for NGC 104 is slightly above their limits while our core value is slightly below. Our total value for NGC 5272 is comparable to that of Hopwood et al. (1999) for 70 K dust. Our value for NGC 5272 is also below that given by Penny et al. (1997) for 80 K dust based on their observations of this cluster at millimeter wavelengths. Our upper limits are above those of Matsunaga et al. (2008) for the five clusters in common, due to the greater sensitivity of their observations.

The dust mass limits we infer are consistent with measurements and upper limits on gas masses. Converting dust masses to gas masses by multiplying by $10^{2-[\text{Fe}/\text{H}]}$, we derive gas masses or upper limits for our sample clusters in the ranges $0.002 - 0.07 M_\odot$ (core) and $0.04 - 1.4 M_\odot$ (total). The only confirmed H I detection, $0.3 M_\odot$ in NGC 7078 (van Loon et al. 2006), is nicely within this range. Our inferred limits on the gas mass are consistent with the results of previous searches for intra-cluster neutral and ionized hydrogen, as summarized in Roberts (1988). Two clusters have reported detections of ionized gas: NGC 104 (Freire et al.

2001) and NGC 1851 (Grindlay & Liller 1977). Freire et al. (2001) derived a total gas mass of $0.1M_{\odot}$ and stated that they expected essentially all the gas in the cluster to be ionized; Grindlay & Liller (1977) estimated the total mass of ionized hydrogen in NGC 1851 as $0.02M_{\odot}$. Our gas mass upper limit for NGC 104 is about the same as the Freire et al. (2001) detection while our upper limit for NGC 1851 is above the Grindlay & Liller (1977) level.

4.2. Expected dust masses

To understand the significance of the dust masses and upper limits derived from the *Spitzer* observations, we need theoretical estimates of the expected dust content of the clusters in the sample. Various estimates of the dust mass within a globular cluster are possible, but little detailed modeling has been done with the exception of the work of Angeletti et al. (1982). Those authors combined dynamical models of star clusters with radiative transfer models to predict dust grain temperatures and luminosities for a few individual clusters, given the presence of $10^{-2}M_{\odot}$ of dust. While it would be valuable to repeat such modeling with modern radiative transfer codes and understanding of dust properties, for present purposes a simpler estimate of globular cluster dust content will suffice. Following Tayler & Wood (1975), the dust mass may be estimated by:

$$\frac{M_d}{M_{\odot}} = \frac{\tau_c}{\tau_{\text{HB}}} N_{\text{HB}} (\delta M) \frac{10^{[\text{Fe}/\text{H}]}}{100} \quad (5)$$

where $\tau_{\text{HB}} = 1.8 \times 10^8$ yr is the horizontal branch lifetime, τ_c is the time since last crossing of the Galactic plane, N_{HB} is the number of stars on the horizontal branch, $(\delta M) = 0.2M_{\odot}$ is the gas mass lost from each star, and $[\text{Fe}/\text{H}]$ is the cluster metallicity. The last factor scales for the change in gas-to-dust ratio with metallicity. Values for τ_c are listed in Table 1; for the two clusters not listed by Odenkirchen et al. (1997) we assume a lower limit of 10^6 yr. To estimate N_{HB} we use the ‘specific evolutionary flux’ method of Renzini & Buzzoni (1986) (see also Evans et al. 2003):

$$N_{\text{HB}} = BL_{\text{bol}}\tau_{\text{HB}} \quad (6)$$

assuming $B = 2 \times 10^{-11}$ stars $\text{yr}^{-1} L_{\odot}^{-1}$ as appropriate for globular clusters, and $L_{\text{bol}} = 2 \times L_V$ (Renzini & Buzzoni 1986) using M_V and $E(B - V)$ given by Harris (1996). For one cluster, we can compare this dust mass estimate to the current dust production rate: Origlia et al. (2007) have recently used *Spitzer* data to identify the mass-losing stars in NGC 104. Summing their mass loss rates for the brightest stars ($M_{\text{bol}} < -2$) and converting to a dust production rate with a gas-to-dust ratio of 200, we estimate $\dot{M}_d = 1.4 \times 10^{-8} M_{\odot} \text{yr}^{-1}$. When multiplied by $\tau_c = 6 \times 10^7$ yr, this yields a total dust content of $0.84M_{\odot}$, about twice that predicted from Eq. 5. The observations of Origlia et al. (2007) are likely to be affected by blending;

correcting for this would lower the inferred dust mass to a value closer to the prediction. Even without such a correction, the comparison gives us confidence that the dust mass predictions are of the correct order of magnitude.

Figure 6 compares the predicted and observed dust masses and upper limits. To augment our sample we analyse additional clusters observed by other groups: NGC 6356² (Hopwood et al. 1998), NGC 6656 (Penny et al. 1997), and NGC 7078 (Boyer et al. 2006), and the six other clusters observed by Matsunaga et al. (2008): NGC 1261, NGC 1904, NGC 2808, NGC 5024, NGC 5139 NGC 5634 and NGC 6402. Where several values for dust mass or upper limits are given in published works, only the one with assumed dust temperature closest to 70 K is used. All of our measurements are well below the predicted values; for most clusters the disagreement is more than an order of magnitude. The same is true for clusters observed by other groups, in that only two clusters have the inferred dust mass close to the predicted value: NGC 6356 (Hopwood et al. 1998) (only for specific assumptions about the dust distribution), and NGC 5634 (Matsunaga et al. 2008), one of the lowest-mass, lowest-metallicity clusters shown. While assuming a lower dust temperature or higher absorption coefficient would increase the dust masses inferred from the observations, it seems unlikely that this can explain the three order of magnitude discrepancy for clusters such as NGC 5272. The other explanation is that one or more of the assumptions involved in Eq. 5 is incorrect: what if globular cluster stars lose much less than $0.2M_{\odot}$ on average, the number of horizontal branch stars does not scale with L_{bol} , the dust-to-gas ratio does not scale with metallicity, or the dust is removed from clusters on a timescale much shorter than the disk passage time τ_c ? Direct observations of red giant mass loss and color-magnitude diagram modeling are consistent with mass losses of approximately $0.2M_{\odot}$ (Origlia et al. 2007; Caloi & D’Antona 2008), and the scaling of N_{HB} with L_{bol} is well-grounded in stellar evolutionary theory. We address the remaining factors below.

With a small sample of clusters, and an even smaller number of low-significance detections, deriving conclusions about the effects of GC properties on mass loss is difficult. Figure 7 shows the dust masses and limits plotted as a function of $[\text{Fe}/\text{H}]$, L_{bol} , τ_c , and $v_{\text{esc},0}$. (In this and the following figure, we plot the more stringent dust mass limits of Matsunaga et al. (2008) for the five clusters in common with our sample.) There are no clear correlations: while the clusters with large inferred dust masses tend to have large τ_c , consistent with the expectation that intracluster dust builds up between cluster passage through the disk, other clusters with similar values of τ_c have much smaller inferred masses.

²For this object we plot the more conservative ‘dust in beam’ mass given by Hopwood et al. (1998); Matsunaga et al. (2008) use the larger ‘dust in core’ value. Regardless of this choice, this cluster still has the largest inferred mass.

This agrees with the finding of Boyer et al. (2006) that the ICM dust in NGC 7078 must have been collecting for a time $t \ll \tau_c$, and with the computation by Matsunaga et al. (2008) that cluster dust lifetimes $\tau_d \ll \tau_c$. The clusters with dust detections do not have the highest central escape velocities, suggesting that possession of a deep potential well is not in itself enough to guarantee the presence of an ICM. The clusters cover a relatively small range in bolometric luminosity; this parameter does not seem to have a strong effect on inferred dust mass.

How does metallicity relate to intracluster dust? The two clusters with the largest inferred dust masses (NGC 7078 and NGC 6356) have the lowest and highest metallicities in the sample. NGC 5024, with a tentative dust detection, also has a low metallicity. The globular cluster data do not help to clarify the controversy over the connection between metallicity and dust production: while some studies show that metallicity and mass loss are not correlated in carbon-rich AGB stars in the Magellanic Clouds (Lagadec & Zijlstra 2008; Sloan et al. 2008), others find that metal-poor carbon stars, like oxygen-rich giants, form less dust (van Loon et al. 2008). The clusters considered here are almost all more metal-poor than the Magellanic Clouds, so their AGB stars are expected to be oxygen, rather than carbon-rich; however the effects (if any) of metallicity on dust mass loss are not evident from the present data.

4.3. Dust removal mechanisms

Observations of mass-losing stars within GCs show that mass loss is occurring at roughly the expected rate, so the non-detection of the ICM means that it must somehow be removed. One possible mechanism is ram-pressure stripping of the cluster ICM by the Galactic halo. Support for this mechanism is provided by detections of diffuse X-ray emission near several Galactic globular clusters (Okada et al. 2007; Krokenberger & Grindlay 1995); Okada et al. (2007) show that the temperature and luminosity of the diffuse emission is consistent with it arising from stripped intracluster gas, and that the energetics require nearly all of the cluster gas to be removed. Those authors also state, to show diffuse X-ray emission, a cluster should have a velocity relative to the Galactic halo $v_h > 150 \text{ km s}^{-1}$. We computed v_h for our sample clusters from the space velocities given in Odenkirchen et al. (1997), Dinescu et al. (1999), or Casetti-Dinescu et al. (2007) assuming a non-rotating halo; these are plotted against dust masses and limits in the left panel of Figure 8. The high velocities of both NGC 7078 and NGC 5024 appear to be problematic for halo stripping; a measurement of the space velocity of NGC 6356 might help to clarify the situation. There is certainly no evidence that clusters with low v_h have more dust; however, the correlation of cluster kinematics with metallicity

combined with any dependence on metallicity of the dust mass limits may also confuse the issue.

Another possible ICM removal mechanism is kinetic energy injected by stellar collisions, as proposed by Umbreit et al. (2008) for M15. Those authors use an N-body model to estimate the time between collisions in the cluster core; their result is of the same order of magnitude as a less-sophisticated estimate based on Eq. 8-125 of Binney & Tremaine (1987):

$$\frac{t_{\text{coll}}}{N} = [7.9 \times 10^{14} \text{ yr}] \frac{\sigma_c}{\rho_0^2 R_c^3} \quad (7)$$

where N is the number of stars within the cluster core (of radius R_c pc), σ_c is the central velocity dispersion in km s^{-1} , and ρ_0 is the central mass density in $M_\odot \text{ pc}^{-3}$. Using the values for R_c , ρ_0 , and $\sigma_c = (2\pi)^{-1/2} r h o_0^{1/3} f_0^{-1/3}$, from King-model fits given in McLaughlin & van der Marel (2005), we computed t_{coll}/N for each cluster in the sample; it is plotted against M_d in the right panel of Fig. 8. Again, there is no clear correlation of the time between collisions and dust masses: while both NGC 6356 and NGC 5024 have long t_{coll} , so do many other clusters. NGC 7078 is core-collapsed and should have a short central collision time. We conclude that neither ram pressure stripping and stellar collisions as the cause of ICM removal can be ruled out by the current data.

5. Conclusions

The intracluster medium of globular clusters remains elusive. Our sample comprised eight Galactic globular clusters thought to have the best chance for retaining an intracluster medium. No significant extended emission is detected from seven of the eight target clusters: any such emission may well be hidden underneath confusion noise from Galactic cirrus. One cluster, NGC 6341, has tentative evidence for excess IR emission from cool dust, although the lack of a $90 \mu\text{m}$ excess casts doubt on the detection. All of our inferred dust masses and upper limits are $< 4 \times 10^{-4} M_\odot$, compared to predicted dust masses ranging from $10^{-0.8} - 10^{-3.6} M_\odot$ for the same clusters. Searches for intracluster gas have been similarly unsuccessful (e.g., van Loon et al. 2006). The lack of intracluster dust and gas implies that either (1) evolved stars in globular clusters make less dust than predicted, or (2) the ICM escapes from the clusters more quickly than expected. The first possibility seems unlikely because of the evidence to the contrary in both NGC 7078 and NGC 5139, where two of the three dustiest, most mass-losing stars have $[\text{Fe}/\text{H}] < -2.0$ (Boyer et al. 2006, 2008).

It is important to point out that ICM escape is not just a trivial occurrence in the life of a globular cluster: substantial mass loss over a GC’s history could affect its dynamical

evolution and perhaps even its survival as a bound system (van Loon & McDonald 2006). Several mechanisms for ICM escape have been discussed above, with energy injected by stellar collisions perhaps being favored over ram pressure from Galactic halo gas. Stellar winds provide another possible mechanism; giant stars with wind velocities above the escape velocity of a typical cluster have been observed (Smith et al. 2004; Dupree et al. 1992). While there is observational evidence that metallicity does not strongly affect the mass loss rate of individual stars (McDonald & van Loon 2007; Sloan et al. 2008), stellar wind velocities do appear to scale with metallicity (Marshall et al. 2004). Faster winds in AGB stars in metal-rich clusters could therefore increase the rate at which the ICM is driven out of the cluster. The existing small sample of clusters does not permit us to distinguish between the possibilities for ICM removal.

Decades of searching have yielded few detections of the elusive globular cluster ICM. A possible strategy for future observations hoping to detect the ICM is to study the removal mechanisms in detail and identify those clusters most likely to retain some ICM. Observations of distant clusters which have had few interactions with the Milky Way could place limits on the importance of halo stripping, although the larger distance of such clusters reduces the effective sensitivity. While infrared facilities available in the near future will not greatly improve on the sensitivity of *Spitzer*, observing a larger sample of clusters would allow a more thorough exploration of the dust content as a function of cluster properties. Observations with future radio facilities such as the Square Kilometer Array will place more stringent limits on the gas content. Together with more sophisticated modeling efforts and detailed examination of mass loss in individual cluster stars, a multi-wavelength observational approach provides the best chance for finding and explaining the elusive intracluster medium in globular clusters.

Facilities: Spitzer (IRAC, MIPS)

We thank the anonymous referee for a careful reading of the manuscript and helpful comments and R.T. Rood for early access to the IRAC data on NGC 6205 and NGC 6341. This work is based on observations made with the *Spitzer Space Telescope*, which is operated by the Jet Propulsion Laboratory, California Institute of Technology under NASA contract 1407. P. B. was partially supported by a Discovery Grant from the Natural Sciences and Engineering Research Council of Canada. M. L. B., C. E. W., E. P., and R. D. G. are supported in part by NASA through *Spitzer* contracts 1276760, 1256406, and 1215746 issued by JPL/Caltech to the University of Minnesota.

REFERENCES

- Alves, D. R., Bond, H. E., & Livio, M. 2000, *AJ*, 120, 2044
- Angeletti, L., Capuzzo-Dolcetta, R., Giannone, P., Blanco, A., & Bussoletti, E. 1982, *MNRAS*, 199, 441
- Binney, J. & Tremaine, S. 1987, *Galactic Dynamics* (Princeton University Press)
- Birkinshaw, M., Ho, P. T. P., & Baud, B. 1983, *A&A*, 125, 271
- Boyer, M. L., McDonald, I., van Loon, J. T., Woodward, C. E., Gehrz, R. D., Evans, A., & Dupree, A. K. 2008, *AJ*, 135, 1395
- Boyer, M. L., Woodward, C. E., van Loon, J. T., Gordon, K. D., Evans, A., Gehrz, R. D., Helton, L. A., & Polomski, E. F. 2006, *AJ*, 132, 1415
- Caloi, V. & D’Antona, F. 2008, *ApJ*, 673, 847
- Carpenter, J. M., Bouwman, J., Silverstone, M. D., Kim, J. S., Stauffer, J., Cohen, M., Hines, D. C., Meyer, M. R., & Crockett, N. 2008, *ApJS*, in press (arXiv:0807.4362)
- Casetti-Dinescu, D. I., Girard, T. M., Herrera, D., van Altena, W. F., López, C. E., & Castillo, D. J. 2007, *AJ*, 134, 195
- Catelan, M. 2000, *ApJ*, 531, 826
- Cohen, J. G., Hsieh, S., Metchev, S., Djorgovski, S. G., & Malkan, M. 2007, *AJ*, 133, 99
- Dinescu, D. I., Girard, T. M., & van Altena, W. F. 1999, *AJ*, 117, 1792
- Dupree, A. K., Sasselov, D. D., & Lester, J. B. 1992, *ApJ*, 387, L85
- Engelbracht, C. W. et al. 2007, *PASP*, 119, 994
- Evans, A., Stickel, M., van Loon, J. T., Eyres, S. P. S., Hopwood, M. E. L., & Penny, A. J. 2003, *A&A*, 408, L9
- Faulkner, D. J., Scott, T. R., Wood, P. R., & Wright, A. E. 1991, *ApJ*, 374, L45
- Fazio, G. G. et al. 2004, *ApJS*, 154, 10
- Forte, J. C., Bassino, L. P., Vega, E. I., Pellizza González, L. J., Cellone, S. A., & Méndez, M. R. 2002, *AJ*, 123, 3263

- Frayser, D. T. et al. 2006, *ApJ*, 647, L9
- Freire, P. C., Kramer, M., Lyne, A. G., Camilo, F., Manchester, R. N., & D’Amico, N. 2001, *ApJ*, 557, L105
- Gehrz, R. D. et al. 2007, *Rev. Sci. Instrum.*, 78, 011302
- Gordon, K. D., Engelbracht, C. W., Rieke, G. H., Misselt, K. A., Smith, J.-D. T., & Kennicutt, Jr., R. C. 2008, *ApJ*, 682, 336
- Gordon, K. D. et al. 2007, *PASP*, 119, 1019
- Grindlay, J. E. & Liller, W. 1977, *ApJ*, 216, L105
- Groenewegen, M. A. T. 2006, *A&A*, 448, 181
- Harris, W. E. 1996, *AJ*, 112, 1487
- Hopwood, M. E. L., Evans, A., Penny, A., & Eyres, S. P. S. 1998, *MNRAS*, 301, L30
- Hopwood, M. E. L., Eyres, S. P. S., Evans, A., Penny, A., & Odenkirchen, M. 1999, *A&A*, 350, 49
- Ita, Y. et al. 2007, *PASJ*, 59, 437
- Jeong, W.-S., Mok Lee, H., Pak, S., Nakagawa, T., Minn Kwon, S., Pearson, C. P., & White, G. J. 2005, *MNRAS*, 357, 535
- Kalirai, J. S., Hansen, B. M. S., Kelson, D. D., Reitzel, D. B., Rich, R. M., & Richer, H. B. 2008, *ApJ*, 676, 594
- Knapp, G. R., Gunn, J. E., & Connolly, A. J. 1995, *ApJ*, 448, 195
- Krockenberger, M. & Grindlay, J. E. 1995, *ApJ*, 451, 200
- Lagadec, E. & Zijlstra, A. A. 2008, *MNRAS*, in press
- Lonsdale, C. J. et al. 2003, *PASP*, 115, 897
- Lynch, D. K. & Rossano, G. S. 1990, *AJ*, 100, 719
- Makovoz, D. & Khan, I. 2005, in *ASP Conf. Ser. 132: Astronomical Data Analysis Software and Systems VI*, ed. P. L. Shopbell, M. C. Britton, & R. Ebert
- Marshall, J. R., van Loon, J. T., Matsuura, M., Wood, P. R., Zijlstra, A. A., & Whitelock, P. A. 2004, *MNRAS*, 355, 1348

- Matsunaga, N., Mito, H., Nakada, Y., Fukushi, H., Tanabé, T. Ita, Y., Izumiura, H., Matsuura, M., Ueta, T., & Yamamura, I. 2008, PASJ, in press (arXiv:0809.2853)
- McDonald, I. & van Loon, J. T. 2007, A&A, 476, 1261
- McLaughlin, D. E. & van der Marel, R. P. 2005, ApJS, 161, 304
- Meszáros, S., Dupree, A. K., & Szentgyörgyi, A. 2008, AJ, 135, 1117
- Nantais, J. B., Huchra, J. P., Barmby, P., Olsen, K. A. G., & Jarrett, T. H. 2006, AJ, 131, 1416
- Odenkirchen, M., Brosche, P., Geffert, M., & Tucholke, H.-J. 1997, New Astronomy, 2, 477
- Okada, Y., Kokubun, M., Yuasa, T., & Makishima, K. 2007, PASJ, 59, 727
- Origlia, L., Ferraro, F. R., Fusi Pecci, F., & Rood, R. T. 2002, ApJ, 571, 458
- Origlia, L., Ferraro, F. R., & Pecci, F. F. 1996, MNRAS, 280, 572
- Origlia, L., Rood, R. T., Fabbri, S., Ferraro, F. R., Fusi Pecci, F., & Rich, R. M. 2007, ApJ, 667, L85
- Penny, A. J., Evans, A., & Odenkirchen, M. 1997, A&A, 317, 694
- Ramdani, A. & Jorissen, A. 2001, A&A, 372, 85
- Reach, W. T. et al. 2005, PASP, 117, 978
- Renzini, A. & Buzzoni, A. 1986, in *Astrophysics and Space Science Library*, Vol. 122, *Spectral Evolution of Galaxies*, ed. C. Chiosi & A. Renzini, 195–231
- Rieke, G. H. et al. 2004, ApJS, 154, 25
- Roberts, M. S. 1988, in *IAU Symposium*, Vol. 126, *The Harlow-Shapley Symposium on Globular Cluster Systems in Galaxies*, ed. J. E. Grindlay & A. G. D. Philip, 411–421
- Rood, R. T. 1973, ApJ, 184, 815
- Sloan, G. C., Kraemer, K. E., Wood, P. R., Zijlstra, A. A., Bernard-Salas, J., Devost, D. & Houck, J.R. 2008, ApJ, in press (arXiv:0807.2998)
- Smith, G. H., Dupree, A. K., & Strader, J. 2004, PASP, 116, 819
- Tayler, R. J. & Wood, P. R. 1975, MNRAS, 171, 467

- Trager, S. C., King, I. R., & Djorgovski, S. 1995, *AJ*, 109, 218
- Umbreit, S., Chatterjee, S., & Rasio, F. A. 2008, *ApJ*, 680, L113
- van Loon, J. T. & McDonald, I. 2006, in *ASP Conf. Ser.*, Vol. 999, Mass loss from stars and the evolution of stellar clusters, ed. A. de Koter, L. Smith, & L. Waters
- van Loon, J. T., Stanimirović, S., Evans, A., & Muller, E. 2006, *MNRAS*, 365, 1277
- van Loon, J. T., van Leeuwen, F., Smalley, B., Smith, A. W., Lyons, N. A., McDonald, I., & Boyer, M. L. 2007, *MNRAS*, 382, 1353
- van Loon, J. T., Cohen, M., Oliveira, J. M., Matsuura, M., McDonald, I., Sloan, G. C., Wood, P. R., & Zijlstra, A. A. 2008, *A&A*, 487, 1055
- Werner, M. et al. 2004, *ApJS*, 154, 1

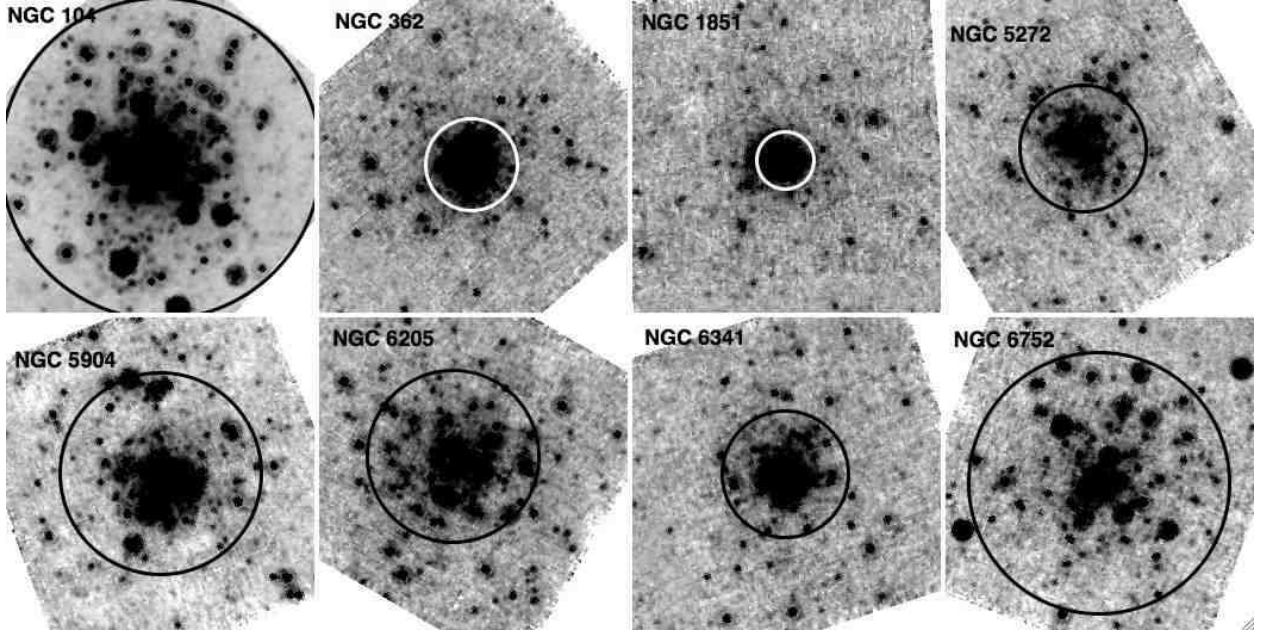


Fig. 1.— MIPS $24\ \mu\text{m}$ images of Galactic globular clusters. Each image is $5.2'$ across, with north up and east to the left. The black or white circles show the half-light radii.

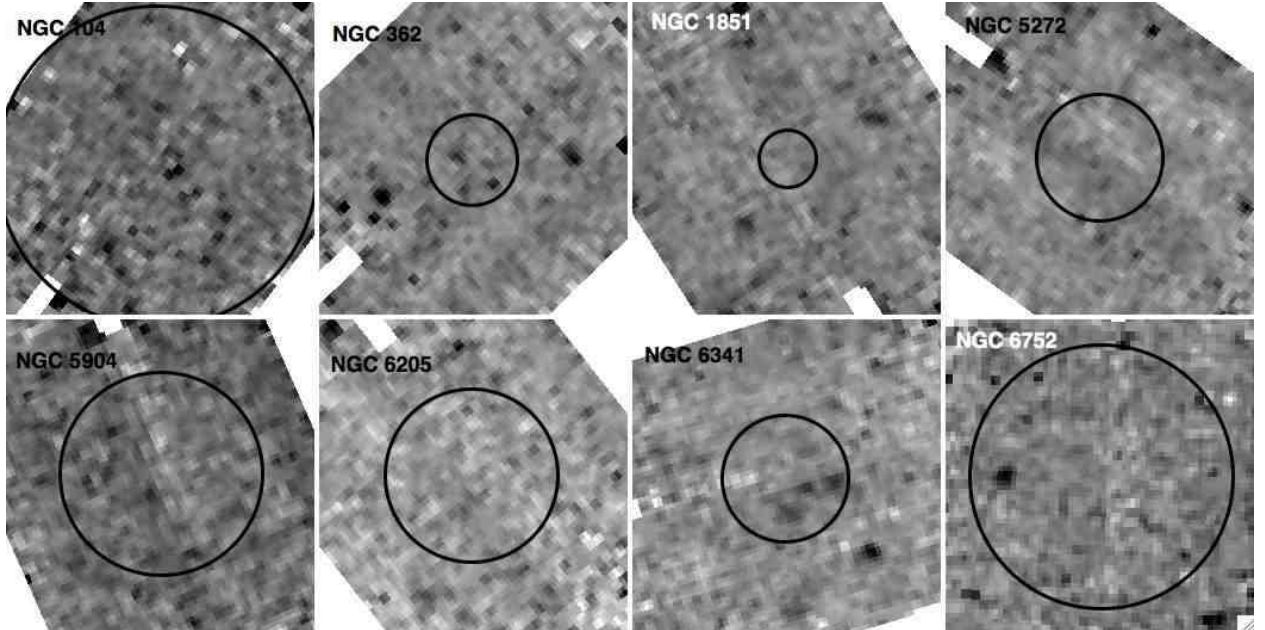


Fig. 2.— MIPS $70\ \mu\text{m}$ images of Galactic globular clusters. Each image is $5.2'$ across, with north up and east to the left. The black circles show the half-light radii (values given in Table 1)

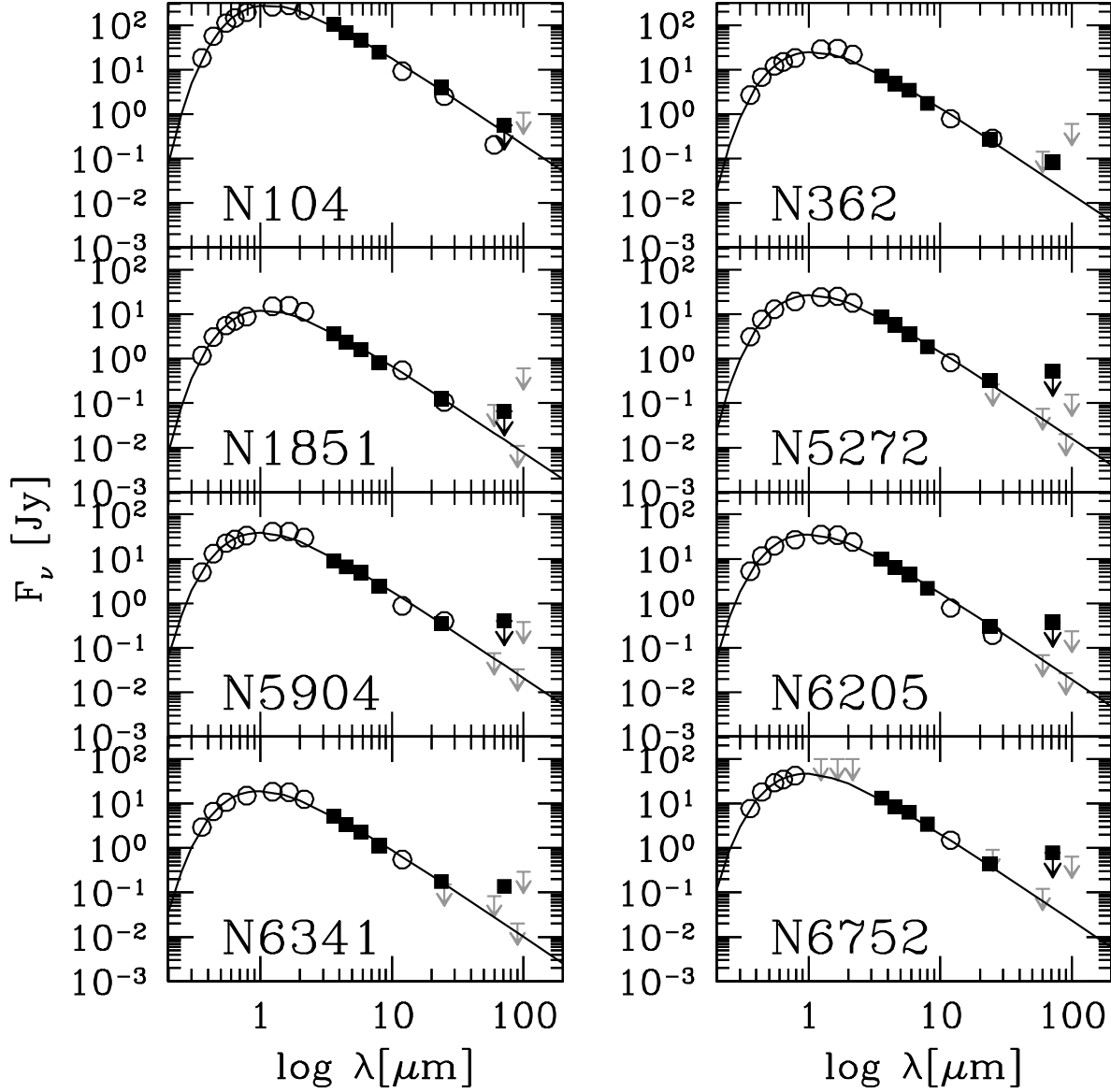


Fig. 3.— Spectral energy distributions of Galactic globular clusters, from 0.3 to 100 μm . Filled symbols are IRAC and MIPS measurements from this work. Open symbols and grey upper limits are published measurements: optical magnitudes from Harris (1996), near-IR magnitudes from Cohen et al. (2007), IRAS Faint Source Catalog measurements from Knapp et al. (1995), and 90 μm upper limits from Matsunaga et al. (2008).

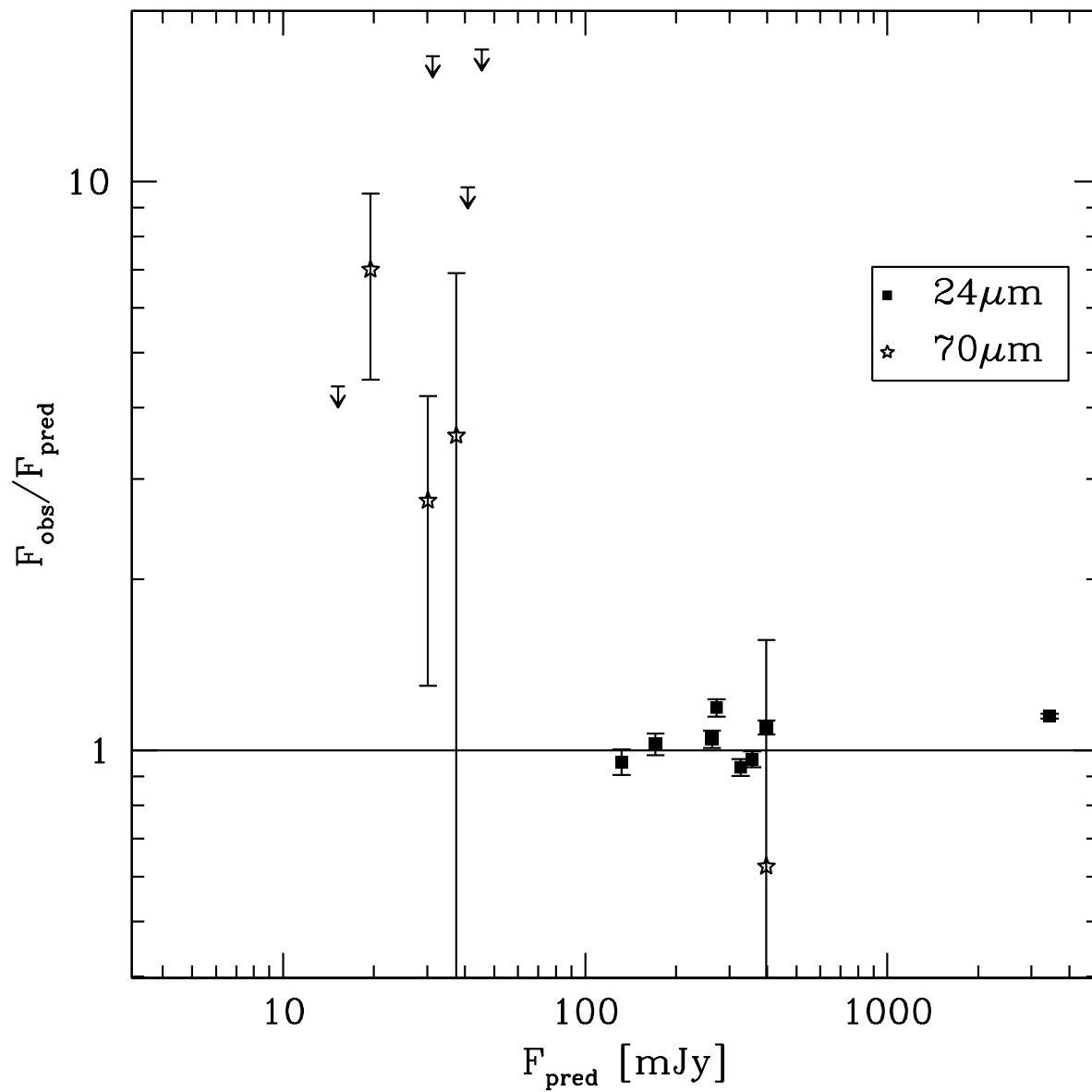


Fig. 4.— Comparison of predicted and measured flux densities for globular clusters at $24\mu\text{m}$ (squares) and $70\mu\text{m}$ (stars and upper limits).

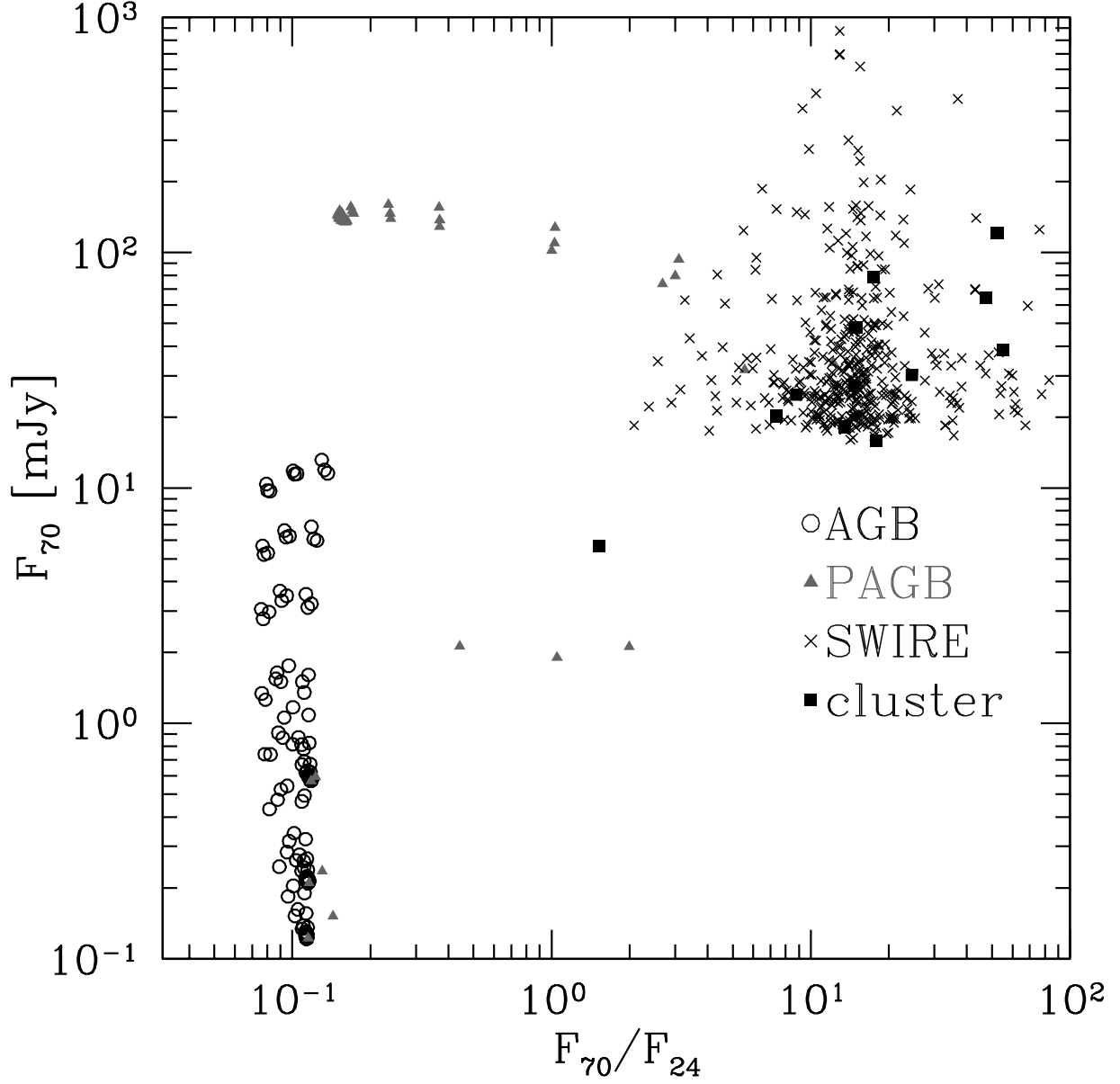


Fig. 5.— MIPS color-magnitude plot for sources detected at 70 μm (squares), AGB star (open circles) and post-AGB star (filled triangles) models from Groenewegen (2006), and SWIRE ELAIS-N2 sources (crosses). The AGB models and cluster source fluxes have been scaled to a distance of 8.5 kpc, assuming the sources to be at the distance of the cluster.

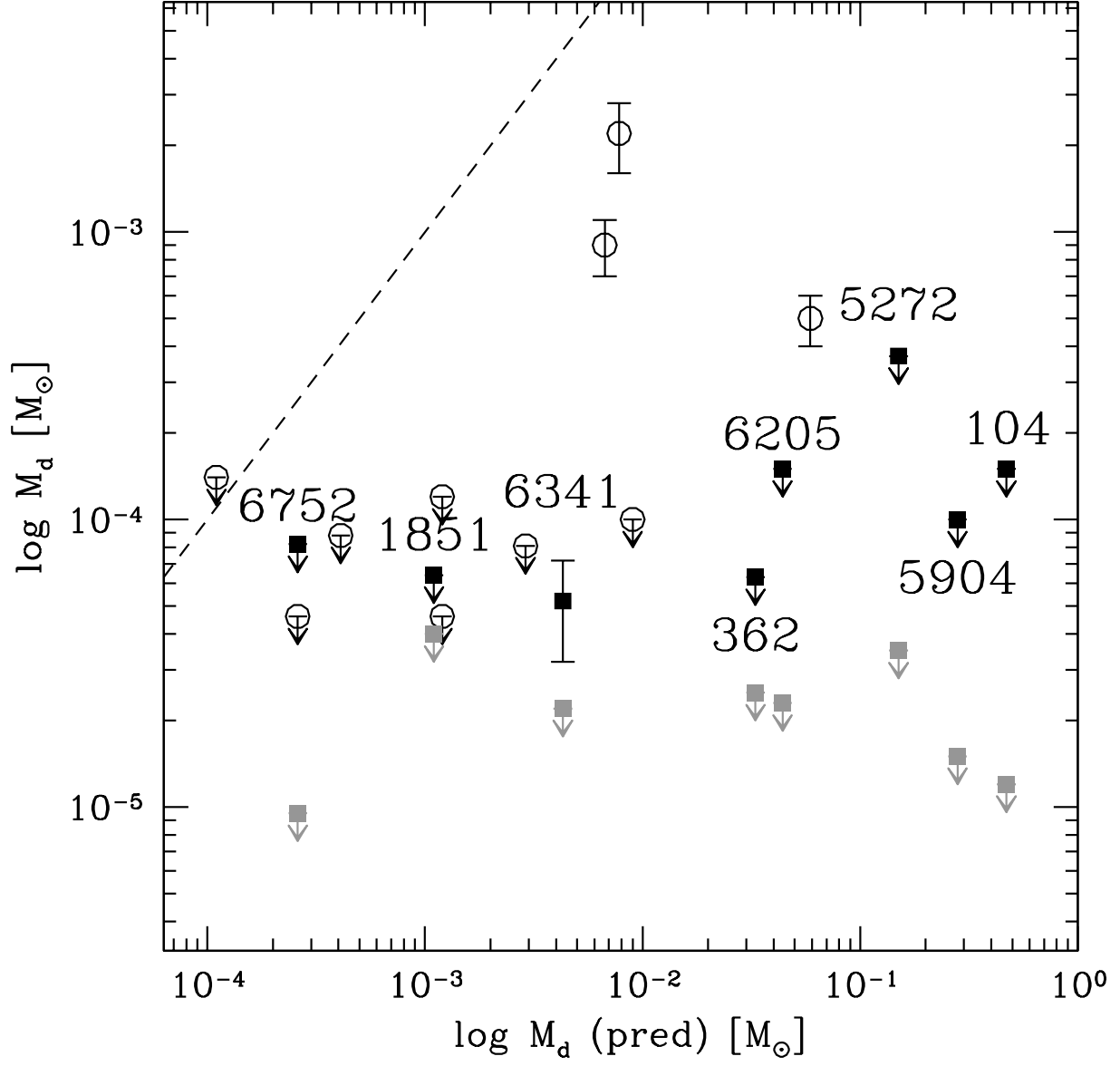


Fig. 6.— Cluster dust masses predicted with Eq. 5 versus derived masses and upper limits from the MIPS observations for both total dust mass (filled black symbols) and core dust mass (filled grey symbols). Previously published dust limits are open symbols, not labeled with cluster NGC number. Dashed line is the line of equality.

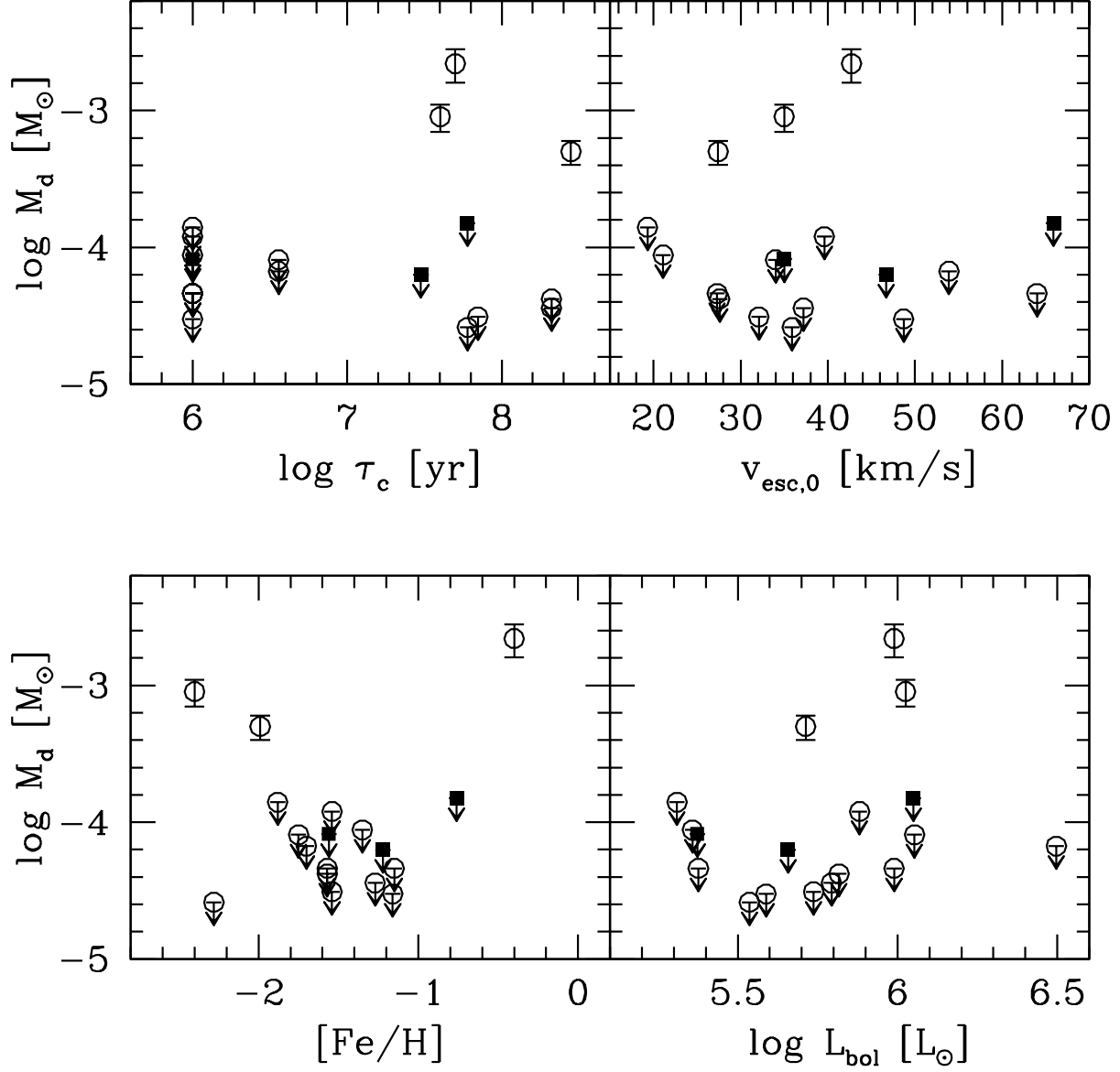


Fig. 7.— Derived cluster dust masses and upper limits versus time since last Galactic disk passage (upper left), central escape velocity (upper right), metallicity (lower left), and bolometric luminosity (lower right). Filled symbols: results from this work (total masses), open symbols: previously published work. An uncertainty of 20% has been assigned to M_d for NGC 5024 as no value was given in the original work (Matsunaga et al. 2008).

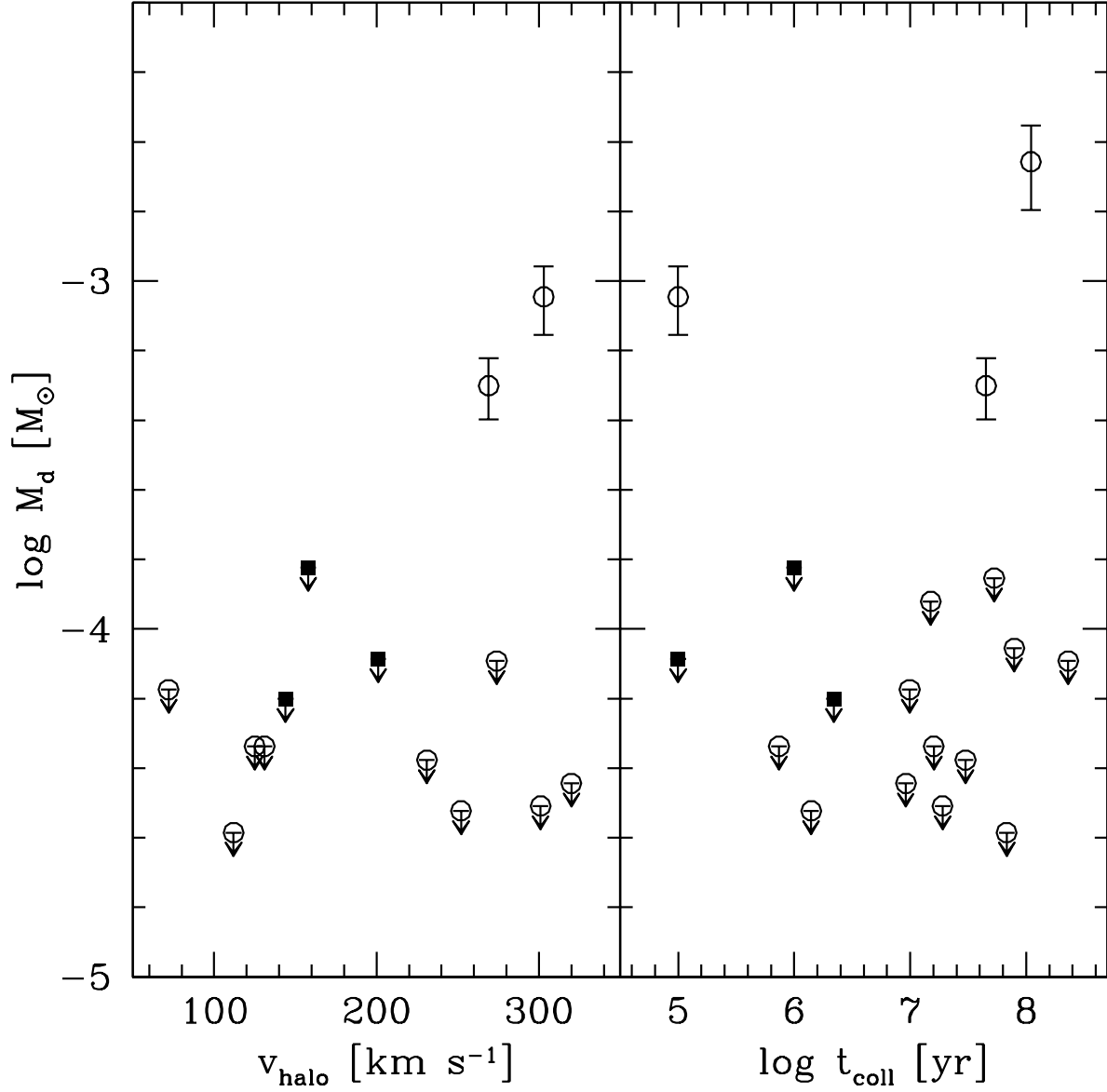


Fig. 8.— Derived cluster dust masses and upper limits versus velocity relative to the halo (left) and estimated time between stellar collisions in the core (right). Symbols as in Fig. 7. In the left panel, clusters NGC 1261, 5646, 6356, and 6402 are not shown, as orbital parameters were not available. In the right panel, both NGC 6752 and NGC 7078 are plotted at $t_{\text{coll}}/N = 10^5$ yr; these clusters are core-collapsed (McLaughlin & van der Marel 2005) and should have short collision times.

Table 1. Globular cluster targets

Target	Distance ^a kpc	[Fe/H] ^a	$v_{\text{esc},0}$ ^b km s ⁻¹	R_h ^b arcsec	L_{bol} ^a L _⊙	τ_c ^c yr
NGC 104 (47 Tuc)	4.5	−0.76	65.9	190.1	1.12×10^6	6×10^7
NGC 362	12.1	−1.22	46.7	49.1	4.54×10^5	3×10^7
NGC 1851	8.5	−1.16	48.7	30.4	3.88×10^5	...
NGC 5272 (M3)	10.4	−1.57	27.6	138.4	6.56×10^5	2.1×10^8
NGC 5904 (M5)	7.5	−1.27	37.2	105.9	6.21×10^5	2.1×10^8
NGC 6205 (M13)	7.7	−1.54	32.1	101.4	5.46×10^5	7×10^7
NGC 6341 (M92)	8.2	−2.28	35.9	61.4	3.44×10^5	6×10^7
NGC 6752	4.0	−1.56	...	114.8	2.36×10^5	...

^aDistance, metallicity and bolometric luminosity from Harris (1996).

^bProjected half-light radius R_h and central escape velocity $v_{\text{esc},0}$ from King-model fits given in McLaughlin & van der Marel (2005) (except R_h for NGC 6752, from Trager et al. 1995).

^cTime since last passage through Galactic disk τ_c , from Odenkirchen et al. (1997).

Table 2. IRAC integrated photometry

Target	$f_\nu(3.6)$ Jy	$f_\nu(4.5)$ Jy	$f_\nu(5.8)$ Jy	$f_\nu(8.0)$ Jy	Dataset ID
NGC 104	107	67.9	46.4	24.7	ADS/Sa.Spitzer#0014502656, ADS/Sa.Spitzer#0007860992
NGC 362	7.10	4.82	3.44	1.73	ADS/Sa.Spitzer#0014503168
NGC 1851	3.57	2.31	1.64	0.82	ADS/Sa.Spitzer#0014503424
NGC 5272	8.67	5.68	3.63	1.85	ADS/Sa.Spitzer#0014504192
NGC 5904	9.25	6.56	4.81	2.42	ADS/Sa.Spitzer#0011586304
NGC 6205	9.66	6.43	4.35	2.17	ADS/Sa.Spitzer#0014504704
NGC 6341	5.05	3.38	2.31	1.16	ADS/Sa.Spitzer#14504960
NGC 6752	13.25	8.41	6.32	3.42	ADS/Sa.Spitzer#14506240

Table 3. MIPS cluster photometry

Target	Center [J2000.0]	half-light		core		Dataset IDs
		$f_{\nu}(24)$ mJy	$f_{\nu}(70)$ mJy	$f_{\nu}(24)$ mJy	$f_{\nu}(70)$ mJy	
NGC 104	00:24:07.4 –72:04:48	1980 ± 18	124 ± 186	91 ± 2	2 ± 9	ADS/Sa.Spitzer#0017315328, ADS/Sa.Spitzer#0017313536
NGC 362	01:03:14.8 –70:50:51	138 ± 5	42 ± 22	29 ± 1.2	5 ± 5	ADS/Sa.Spitzer#0017316352, ADS/Sa.Spitzer#0017314560
NGC 1851	05:14:06.8 –40:02:49	63 ± 3	-7 ± 11	20 ± 1	-1 ± 4	ADS/Sa.Spitzer#0017316096, ADS/Sa.Spitzer#0017314048
NGC 5272	13:42:11.6 +28:22:47	161 ± 6	1 ± 87	10 ± 0.7	-2 ± 5	ADS/Sa.Spitzer#0017316608, ADS/Sa.Spitzer#0017314816
NGC 5904	15:18:33.0 +02:04:50	172 ± 6	-34 ± 67	14 ± 0.8	-9 ± 5	ADS/Sa.Spitzer#0017313024, ADS/Sa.Spitzer#0017312768
NGC 6205	16:41:39.9 +36:27:28	153 ± 5	67 ± 62	9 ± 0.6	-1 ± 6	ADS/Sa.Spitzer#0017315584, ADS/Sa.Spitzer#0017313792
NGC 6341	17:17:07.8 +43:08:11	88 ± 4	68 ± 25	13 ± 0.8	-1 ± 5	ADS/Sa.Spitzer#0017315840, ADS/Sa.Spitzer#0017314304
NGC 6752	19:10:52.0 –59:59:02	218 ± 6	-5 ± 129	13 ± 0.8	-4 ± 9	ADS/Sa.Spitzer#0017315072, ADS/Sa.Spitzer#0017313280

Note. — All uncertainties are 1σ .

Table 4. Non-stellar 70 μ m fluxes and inferred dust masses

Target	$f_{70,\text{tot}}$ mJy	$f_{70,\text{core}}$ mJy	M_{pred} M_{\odot}	M_{total} M_{\odot}	M_{core} M_{\odot}
NGC 104	-75 ± 186	-15 ± 9	4.7×10^{-1}	$< 1.5 \times 10^{-4}$	$< 1.2 \times 10^{-5}$
NGC 362	26 ± 22	3 ± 5	3.3×10^{-2}	$< 6.3 \times 10^{-5}$	$< 2.5 \times 10^{-5}$
NGC 1851	-14 ± 11	-6 ± 4	$> 1.1 \times 10^{-3}$	$< 6.4 \times 10^{-5}$	$< 4 \times 10^{-5}$
NGC 5272	-15 ± 87	-6 ± 5	1.5×10^{-1}	$< 3.7 \times 10^{-4}$	$< 3.5 \times 10^{-5}$
NGC 5904	-54 ± 67	-18 ± 6	2.8×10^{-1}	$< 1.0 \times 10^{-4}$	$< 1.5 \times 10^{-5}$
NGC 6205	48 ± 62	-4 ± 6	4.4×10^{-2}	$< 1.5 \times 10^{-4}$	$< 2.3 \times 10^{-5}$
NGC 6341	59 ± 25	-4 ± 5	4.3×10^{-3}	$(5.2 \pm 2.2) \times 10^{-5}$	$< 2.2 \times 10^{-5}$
NGC 6752	-28 ± 129	-10 ± 9	$> 2.6 \times 10^{-4}$	$< 8.2 \times 10^{-5}$	$< 9.5 \times 10^{-6}$